The mean suspended sediment concentration profile of silty sediments under wave-dominant conditions

Zuo, Liqin; Roelvink, Dano; Lu, Yongjun

DOI
10.1016/j.csr.2019.07.016

Publication date
2019

Document Version
Accepted author manuscript

Published in
Continental Shelf Research

Citation (APA)
Zuo, L., Roelvink, D., & Lu, Y. (2019). The mean suspended sediment concentration profile of silty sediments under wave-dominant conditions. *Continental Shelf Research*, *186*, 111-126. https://doi.org/10.1016/j.csr.2019.07.016

The mean suspended sediment concentration profile of silty sediments under wave-dominant conditions

Liqin Zuo [a, b, d], Dano Roelvink [b, c, d*], Yongjun Lu[a*]

[a] State Key Laboratory of Hydrology-Water Resources and Hydraulic Engineering, Nanjing Hydraulic Research Institute, 210024 Nanjing, China
[b] IHE Delft Institute for Water Education, Delft, the Netherlands
[c] Deltares, Delft, The Netherlands
[d] Civil Engineering and Geosciences Faculty, Delft University of Technology, Delft, The Netherlands

ABSTRACT

Suspended sediment concentration (SSC) is one of the fundamental topics in sediment study. The parameterization of the SSC profile of silty sediments is still under-researched. This study focuses on the mean SSC profile for silty sediments under non-breaking wave-dominant conditions. First, inspired by a 1DV model, different types of the distribution of mean eddy viscosity were proposed, i.e., a toe-type distribution over flat bed and a constant-toe type distribution over rippled bed. Then, the time-averaged diffusion equation for suspended sediment transport was analytically solved, and expressions for the mean SSC profiles were derived. The expressions involve several basic physical processes, including the effects of bed forms, stratification, hindered settling and mobile bed. Verification using a number of experimental datasets showed that the proposed expressions can properly calculate the mean SSC for silt and are applicable for sand as well. In conclusion, this research provides an approach to estimate the mean SSC for silty sediments under wave-dominant conditions, which is expected to be applicable for engineering practice and numerical modelling.

Key words: sediment concentration profile; eddy viscosity; sediment diffusivity; silty sediment; rippled bed; flat bed

1. Introduction

Sediment transport is a key issue in coastal evolution and utilization. On the basis of grain size d, sediments can be simply classified as gravel (d > 2 mm), sand (d = 62 μm~2 mm), silt (d = 4-62 μm), and clay (d < 4 μm) (van Rijn, 1993). Silt-dominant coastal areas can be found, for example the eastern and southwestern Bohai Bay, the Jiangsu coast in China and the Semen Tuban

* Corresponding author.
Email address: lqzuo@nhri.cn (Liqin Zuo), d.roelvink@un-ihe.org (Dano Roelvink) , yjlu@nhri.cn (Yongjun Lu)

port sea area in Indonesia. Meanwhile, silt is the prevailing sediment fraction in some rivers, such as the Yellow River and Yangtze River in China (Te Slaa et al., 2015). Recent field observations and flume experiments have shown that silty sediment or silt-dominant sediment has a special behaviour, which is neither like typical sand (non-cohesive) nor like typical mud (cohesive). Erosion tests have suggested that silt-enriched mixtures exhibit cohesive-like behaviour (Roberts et al., 1998), but flocculation has not been observed in settling experiments on silt (with clay contents less than 10%) (Te Slaa et al., 2013; Te Slaa et al., 2015; Yao et al., 2015).

According to laboratory experiments in combination with field work in silt-rich environments (Te Slaa et al., 2013), when the clay content is larger than 5-10%, the sediment mixtures behave as cohesive sediment. Mehta and Lee (1994) suggested that the 10-20 μm size may be considered practically to be the dividing size that differentiates cohesive and cohesionless sediment behaviour. Stevens (1991) proposed 16 μm to be the division between sediments that flocculate significantly. Some experiments (Li, 2014; Yao et al., 2015; Zhou and Ju, 2007) showed that sediments with grain size of 45 μm to 110 μm shared similar suspension phenomenon, i.e. a high concentration layer was found under wave-current conditions. Some scholars defined the coast with sediment medium grain size of 30 μm to 125 μm and the clay percentage less than 25% as silty coast, to be differentiated with sandy coast and muddy coast (Cao et al., 2009). Thus, this study focuses on silt and very fine sand, defined as silty sediment, which is considered to be the transition zone of non-cohesive and cohesive sediments. The latter two types of sediments have been studied extensively; however, the behavior of silt-dominant sediment is still poorly understood (Van Maren et al., 2009). Silty sediment has drawn much attention in recent years, such as studies on the hindered settling (Te Slaa et al., 2015), sediment movement (Cao et al., 2009) and reference concentration (Yao et al., 2015).

For engineering practice or 2D/3D numerical simulation, it is imperative to know the expressions of the time-averaged SSC profile. However, parameterization for silty sediments remains understudied. Since the early 1900s, many scholars have studied the expressions for sand's SSC profile, but few investigated silty sediments (Jayaratne et al., 2011; Liu, 2007; Nielsen, 1992; Nielsen, 1995; Rouse, 1937; Sleath, 1982; van Rijn, 2007; Winyu and Shibayama, 1995; Zheng et al., 2013). To develop a complete set of time-averaged suspended sediment concentration models or expressions has been a challenging task, due to the complexity of the suspension mechanism (Jayaratne et al., 2015). The SSC profile is often described as an expression of a reference

concentration and a shape function (Bolaños et al., 2012). The reference concentration, which has been studied extensively by many scholars, is specified close to the bed and provides the absolute level of the suspended load (Nielsen, 1992; van Rijn, 2007; Zyserman and Fredsøe, 1994). The shape function represents the distribution profile with height above the bed and is normally derived from the sediment diffusivity distribution. Commonly, three kinds of sediment diffusivity distribution are known (i.e., uniform, linear and parabolic), which induce different types of sediment concentration profile (i.e., exponential, power and Rouse, respectively) (Soulsby, 1997). Many formulas for sediment concentration profile were proposed through assuming sediment diffusivity distribution (Coleman, 1969; Lundgren, 1972; Ravindra Jayaratne and Shibayama, 2007; Rouse, 1937; Umeyaina, 1992; van Rijn, 1993; Winyu and Shibayama, 1995). Nielsen (1992, 1995) argued that pure gradient diffusion was unsatisfactory and proposed a combined convection diffusion model by introducing a sediment mixing length and a convective function.

Previous studies on sand sediment concentration profile provide the methodology for further studying silty sediment. This study aims to parameterize the sediment concentration profile of silt and very fine sand sediments under non-breaking, wave-dominant conditions. Firstly, distributions of wave-related sediment diffusivity over different bed forms were proposed inspired by a 1DV model; then, the time-averaged diffusion equation for suspended sediment was analytically solved by considering several important physical processes. This study is expected to assist in better understanding the SSC profile of silt and very fine sand as well as providing approaches for 3D models. This paper is organized as follows: Section 1 is the introduction; Section 2 provides a description of the methodology and data collection; Section 3 presents the expression and verification of the SSC profile over flat bed; Section 4 presents the expression and verification of the SSC profile over rippled bed; Section 5 is discussion; and Section 6 contains the summary and concluding remarks.

2. Derivation and Materials

2.1. Derivation method

The classic time-averaged governing equation for suspended sediment transport can be solved analytically to obtain the vertical distribution of SSC,

$$w_s \bar{c}(z) + \varepsilon_s \frac{d\bar{c}(z)}{dz} = 0 \tag{1}$$

89 in which w_s is settling velocity, ε_s is sediment diffusivity coefficient, $\bar{c}$ is mean sediment
90 concentration and *z* is vertical coordinate.

91 The particular solution to Eq. (1):

92 $$\bar{c}(z) = \overline{c_a} e^{-G(z)} \text{ with } G(z) = \int_{z_a}^{z} \frac{w_s}{\varepsilon_s(z)} dz \quad (2)$$

93 in which, $\overline{c_a}$ is the time-averaged reference concentration at reference height z_a. This solution
94 depends on $\overline{c_a}$ and the distribution of sediment diffusivity $\varepsilon_s(z)$.

95 *2.2 Sediment diffusivity*

96 The sediment diffusivity ε_s is normally related to eddy viscosity υ_t with $\varepsilon_s = \upsilon_t / \sigma$, in
97 which σ is Prandtl-Schmidt number. The value of σ is still in argument. In some models, σ was
98 assumed to be 1 and got fairly good predictions (e.g., Li and Davies, 1995; Guizien et al., 2003;
99 Zhang et al., 2011). van Rijn (1993) indicated that σ is generally smaller than unity for fine
100 suspended sediments on the basis of laboratory experiments with steady uniform flow. The value
101 of 0.7-2.0 was used by Winterwerp (2006). However, there is still no universal value of the Prandtl-
102 Schimidt number because of complex two-phase interactions. In this paper, the strategy is that first
103 we assume σ = 1, then the sediment diffusivity is modified by van Rijn (2007)'s damping
104 coefficient considering the stratification effects, which will be presented in details in subsection
105 2.3.3.

106 Based on an intra-wave 1DV model for wave-current bottom boundary layer, the wave-
107 related eddy viscosity over different bed forms was studied (Zuo et al., 2018). The 1DV model
108 was established for flow-sediment dynamics in the wave-current bottom boundary layer, especially
109 for simulation of the high concentration layer of silt and very fine sand. Based on physical
110 background, special approaches for sediment movement were introduced, including approaches
111 for different bed forms (rippled bed and flat-bed), hindered settling, stratification effects, mobile
112 bed effects, reference concentration and critical shear stress. Ripples exhibiting the formation of
113 fluid vortices (orbital excursion larger than ripple length) are called vortex ripples (Bagnold and
114 Taylor, 1946). The term 'flat bed' is used to refer to 'dynamically plane' rough beds, including sheet
115 flow conditions and rippled beds of mild steepness (< 0.12) (Davies and Villaret, 2002), above
116 which momentum transfer occurs via turbulent processes rather than vortices. Under flat bed

conditions, the normal k- ε turbulence model is employed. For rippled beds, the combined vortex and k-ε model was employed to simulate the turbulence and the k and ε values at the interface of the vortex-dominant layer were derived. Please see the literature (Zuo et al., 2018) for more details.

Fig. 1 and Fig. 2 show the intra-wave process of velocity profiles, eddy viscosity profiles and sediment concentration profiles simulated by the model. It can be seen that the distribution of eddy viscosity is different over flat bed and vortex rippled bed. The feedback interactions between the hydrodynamics, bed forms and sediment properties were investigated by some researchers (Soulsby, 1997; Thorne and Hanes, 2002; Nielsen, 1995). The presence of bed forms modifies the bottom stress, near-bed turbulence and sediment entrainment; these processes in turn induce different bed-form patterns. Here, the expressions of time-averaged wave-related sediment diffusivity/eddy viscosity were proposed for flat bed and vortex rippled bed, inspired by the results of the 1DV model. As a result, different expressions of sediment concentration profile over different bed forms were derived.

For silt, the effects of bed forms are important since the bed forms transform easily. Normally, the criterion of bed forms can be represented by the mobility number $\psi = u_{wc}^2/[(s-1)gd_{50}]$, where u_{wc} = the velocity of combined wave-current, $u_{wc}^2 = u_m^2 + u_c^2$, u_m = maximum wave orbital velocity, u_c = current velocity, s = 2.65 = relative density, g = gravity acceleration, and d_{50} = median grain size. According to O'Donoghue et al. (2006), flat bed (sheet-flow) regime prevails when $\psi > 300$, the ripple regime happens when $\psi < 190$ and a transition regime prevails when $190 < \psi < 300$. Fig. 3 shows the criterion conditions of bed forms according to d_{50} and wave orbital velocity. It can be seen that, silt may experience both rippled bed and sheet flow under moderate conditions (bed type may change when u_m = 0.30-0.38 m/s for d_{50} = 30 μm). It has to be mentioned that bed forms only serve as bed conditions. We do not penetrated into the sheet flow layer, which is another topic. This paper focuses on suspended sediment concentration above the reference height. Different approaches of sediment diffusivity as well as bed roughness over different bed forms are employed.

It has to be mentioned that, O'Donoghue et al. (2006)'s criterion was derived from the datasets of sandy sediments, and a thorough study on the criterion of bed types for silt needs further study. Besides O'Donoghue et al. (2006)'s criterion, we also take the ripple steepness into account. The vortex ripples are limited with ripple steepness larger than 0.12; for the lower ripple steepness,

the bed form is hydrodynamically plane (Davies and Thorne, 2005; van der Werf et al., 2006) and this kind of rippled bed is treated as 'flat bed'. In practice, the vortex rippled bed is judged as $\psi < 300$ and $\eta / \lambda \geq 0.12$, in which η is ripple height and λ is ripple length, while for flat bed the criterion is $\psi \geq 300$ or $\eta / \lambda < 0.12$.

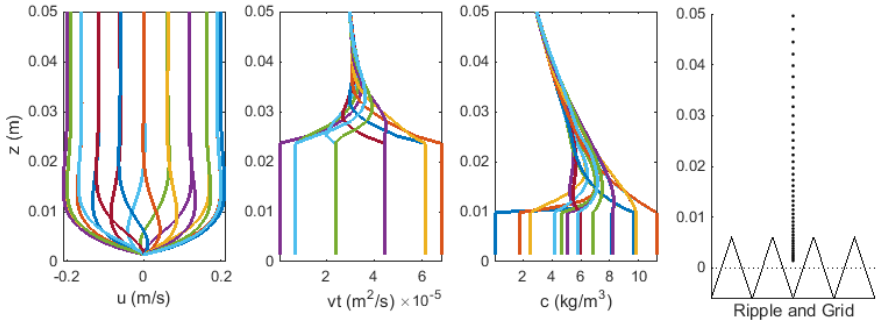

Fig. 1. Intra-wave process of velocity profiles (left column), eddy viscosity profiles (middle column) and sediment concentration profiles (right column) over rippled bed calculated by the 1DV model (The calculation conditions: water depth h=0.3 m, maximum wave orbital velocity u_m = 0.2 m/s, wave period T = 3 s and d_{50} = 0.062 mm)

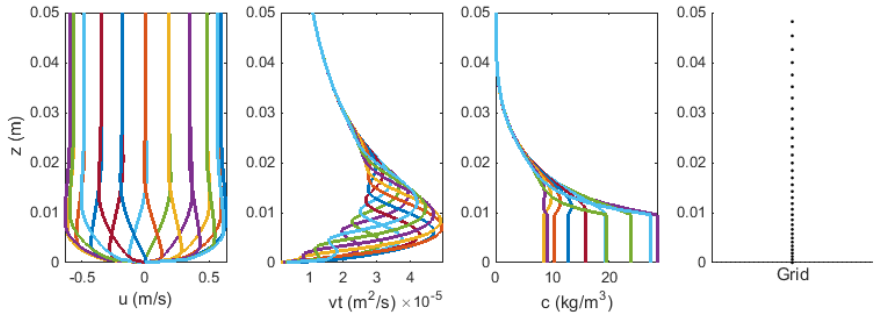

Fig. 2. Intra-wave process of velocity profiles (left column), eddy viscosity profiles (middle column) and sediment concentration profiles (right column) in plane bed conditions calculated by the 1DV model (The calculation conditions: h = 0.3 m, u_m = 0.6 m/s, T = 3 s and d_{50} = 0.062 mm)

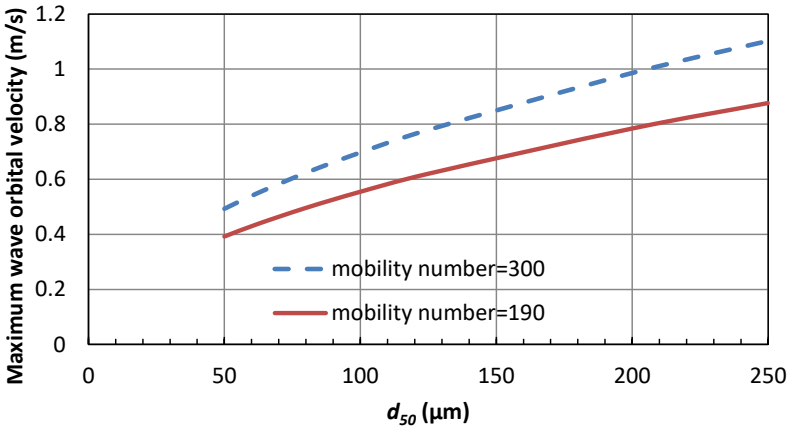

Fig. 3. The criterion conditions of bed forms according to d_{50} and the maximum wave orbital velocity u_m (extrapolated by O'Donoghue et al. (2006)'s criterion)

2.2.1. The wave-related mean sediment diffusivity over flat bed

Many turbulence models can well simulate the eddy viscosity instantaneously, such as the *k*-ε model. However, for analytical analysis, the time-averaged distribution of eddy viscosity has to be parameterized. A toe-type distribution of the phase-averaged wave-related eddy viscosity was proposed in non-breaking wave conditions (Fig. 1), according to the results of the 1DV model (Zuo et al., 2018). The eddy viscosity can be described by a three-layer distribution, see Eq. (3), i.e., linear at the lower BBL (bottom boundary layer), parabolic at the middle part and uniform at the upper part:

$$\upsilon_t(z)=\begin{cases}\kappa u_*' z & z\le 0.5\delta_w \\ \kappa u_*' z(a-bz/2.5\delta_w) & 0.5\delta_w < z < 2.5\delta_w \\ \beta_s \kappa u_*' \delta_w & z\ge 2.5\delta_w\end{cases} \tag{3}$$

in which, κ = 0.4 = Karman number, $u_*' = 0.5\,u_{*w}$ = effective mean wave shear velocity, u_{*w} = wave maximum shear velocity, $\delta_w = \kappa u_*/\omega$ = thickness of wave boundary layer (Grant and Madsen, 1986), ω = wave frequency, β_s, *a* and *b* are coefficients with $\beta_s = 0.8$, *a* =1.17 and *b* = 0.85.

Fig. 4 shows the comparison of the eddy viscosity computed by Eq. (3) with the results from the 1DV model. It can be seen that, the proposed distribution of eddy viscosity has similar tendency with the results of the 1DV model, though there are deviations in the upper part in different cases. Then, the sediment diffusivity is obtained by $\varepsilon_s = \upsilon_t/\sigma$.

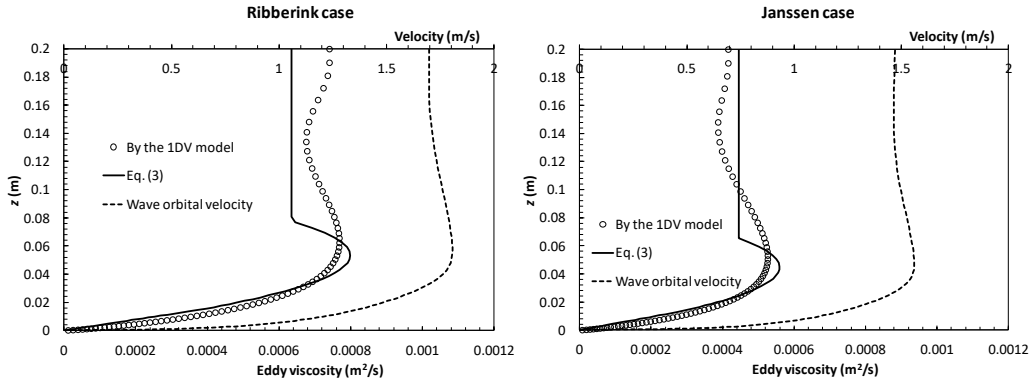

Fig. 4. Comparison of the calculated mean eddy viscosity distribution with the results of the 1DV model (the wave conditions were after Dohmen Janssen et al. (2001) and Ribberink and Al-Salem (1995))

2.2.2. The wave-related mean sediment diffusivity over rippled bed

Over rippled bed, momentum transfer and the associated sediment dynamics in the near-bed layer are dominated by coherent motions, in particular the process of vortex formation above the ripple lee slopes and the shedding of these vortices at times of flow reversal (van der A, 2005). In a near-bed layer, approximately two ripple heights below, the flow dynamics are dominated by the coherent periodic vortex structures, whereas above this layer the coherent motions break down and are replaced by random turbulence (Davies and Villaret, 1999). According to this physical background, a two-layer model was adopted, see Fig. 5, i.e., the vortex-dominant layer at the bottom and the turbulence-dominant layer above, separated by twice the ripple height (Davies and Thorne, 2005; van der Werf et al., 2006).

In the vortex layer ($z<2\eta$), Nielsen (1992)'s formula was employed for the eddy viscosity, which was also referred by Davies and Thorne (2005),

$$\upsilon_t(z) = \overline{\upsilon_{tN}} = c_{vor} A\omega k_s \qquad z<2\eta \tag{4}$$

in which, c_{vor} = 0.004-0.005, A is wave amplitude, ω is wave frequency, and k_s is roughness height.

Above the vortex layer ($z>2\eta$), a toe-type mean eddy viscosity was employed (Eq. 5), with linear distribution at the bottom, parabolic distribution in the middle part and uniform in the upper part, which is similar to the flat bed. According to the comparison with the results of the 1DV model, Fig. 6 shows that the proposed distribution has similar tendency with the results of the 1DV model, though there are deviations in the upper part.

$$\upsilon_t(z)=\begin{cases}\kappa u_{v*} z & 2\eta < z \le 2.5\eta \\ \kappa u_{v*} z[a_r - b_r z/4.5\eta] & 2.5\eta < z \le 4.5\eta \\ b_{up}\kappa u_{v*}\eta & z > 4.5\eta\end{cases} \quad (5)$$

in which $u_{v*} = \overline{\upsilon_{tN}} / \kappa / 2\eta$, a_r = 1.625, b_r = 1.125 and b_{up} = 2.25.

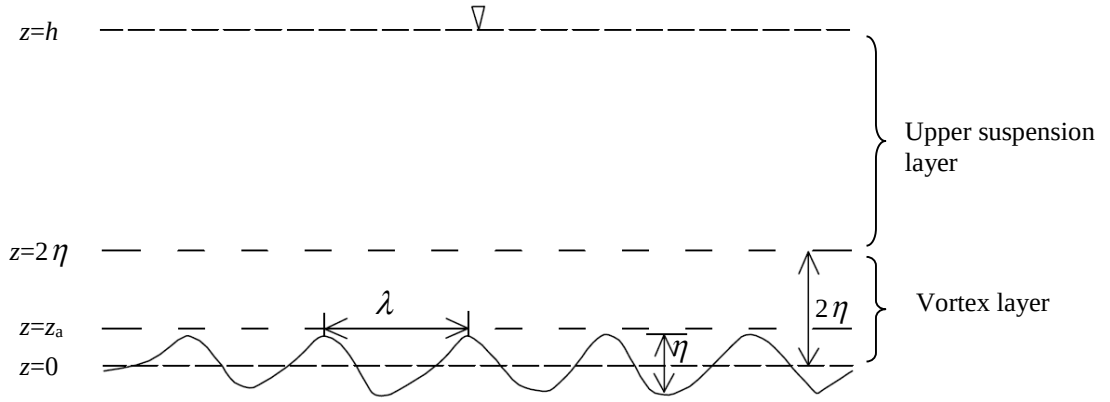

Fig. 5. The physical concept of a two-layer model over rippled bed (*h* is water depth)

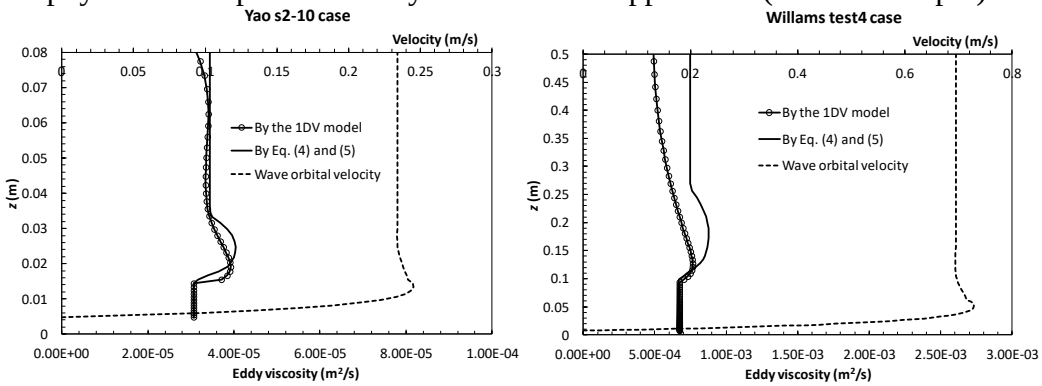

Fig. 6. Comparison of the calculated mean eddy viscosity with the results of the 1DV model (The wave conditions were after Yao et al. (2015) and Williams et al. (1998))

The sediment diffusivity in the lower layer above rippled beds is significantly larger than the eddy viscosity, with $\varepsilon_s = \beta\upsilon_t / \sigma$ (Nielsen, 1992; Thorne et al., 2002). The coefficient β is given by

$$\beta=\begin{cases}4 & z \le 2\eta \\ 4-3\left(\dfrac{z-2\eta}{h-2\eta}\right)^{\gamma} & z > 2\eta\end{cases} \quad (6)$$

with the coefficient γ = 0.4-1.

2.2.3. The sediment diffusivity under combined wave-current conditions

Under combined wave-current conditions, the combined sediment diffusivity is given by a square sum of the wave-related and current-related diffusivities (Nielsen, 1992; van Rijn, 2007).

$$\varepsilon_{s,cw} = \sqrt{\varepsilon_{s,c}{}^2 + \varepsilon_{s,w}{}^2} \tag{7}$$

in which $\varepsilon_{s,cw}$ = combined sediment diffusivity coefficient, $\varepsilon_{s,w}$ = wave-related sediment diffusivity coefficient, and $\varepsilon_{s,c}$ = current-related sediment diffusivity coefficient.

van Rijn (2007)'s formula is employed for the current-related sediment diffusivity,

$$\varepsilon_{s,c} = \begin{cases} \kappa\beta_c u_{*c} z(1 - z/h) & z \le 0.5h \\ 0.25\kappa\beta_c u_{*c} h & z > 0.5h \end{cases} \tag{8}$$

in which u_{*c} = current-related shear velocity, and $\beta_c = \max[1.5, 1 + 2(w_s / u_{*c})^2]$.

2.3. Key approaches for silty sediments

2.3.1. Reference concentration

The reference concentration $\overline{c_a}$ for silt was employed (Yao et al., 2015), which was originally proposed by van Rijn (2007) and was extended to silt range by Yao et al. (2015).

$$\overline{c_a} = \beta_y (1 - p_{clay}) f_{silt} \frac{d_{50}}{z_a} \frac{T_*^{1.5}}{D_*^{0.3}} \tag{9}$$

in which $\beta_y = 0.015$ is an original empirical coefficient for sand, and Yao et al. (2015) extended it to silt by using $\beta_y = 0.118 D_*^{-0.7}$, with a maximum value of 0.118 and a minimum value of 0.015. $f_{silt} = d_{sand} / d_{50}$ is the silt factor ($f_{silt} = 1$ for $d_{50} > d_{sand}$), and d_{sand} = 62 μm. p_{clay} is the percentage of clay material in the bed. $D_* = d_{50}[(s-1)g/\upsilon^2]^{1/3}$ is the dimensionless particle size. $T_* = (\tau' - \tau_c)/\tau_c$, in which τ' is originally the time-averaged effective bed-shear stress under currents and waves. τ_c is the critical bed shear stress. The reference height z_a follows Yao et al. (2015), which is defined as the maximum value of half the wave-related and half the current-related bed roughness values, with a minimum value of 0.01 m.

2.3.2. Critical shear stress for sediment threshold

In the above formulas, the critical shear stress needs to be determined and generally the Shields curve can be employed. However, the Shields curve which is normally used for non-

cohesive sediments cannot be used for silt. An expression of silt-sand incipience motion was employed here, which considered the cohesive force and additional static water pressure for fine sediment (Zuo et al., 2017).

$$\theta_{zc}=\begin{cases}0.025\,\mathrm{Re}\,d_*^{-0.07} & \mathrm{Re}\,d_*<1\\ 0.00543\ln(\mathrm{Re}\,d_*)+0.025 & 1\le \mathrm{Re}\,d_*\le 100\\ 0.05 & \mathrm{Re}\,d_*>100\end{cases} \tag{10}$$

where $\theta_{zc}=\dfrac{\tau_c}{\rho(s-1)gd+a_z\beta_z\rho\dfrac{\varepsilon_k+gh\delta_s\sqrt{\delta_s/d}}{d}}$; $\mathrm{Re}\,d_*=\dfrac{d}{4\upsilon}\sqrt{(s-1)gd}$ is the non-dimensional sand Reynolds number; ε_k = 1.75×10^{-6} m^3/s^2 is the cohesive force coefficient; δ_s = 2.31×10^{-7} m is the bound water thickness; ρ is the water density; d is sediment grain size; a_z = 0.19 is a coefficient; υ is the kinematic viscosity coefficient, and β_z is the compaction coefficient, normally $\beta_z=1$ for well-compacted sediments.

2.3.3. Stratification effects

In turbulence models, the buoyancy flux can be introduced to simulate the stratification effects. However, to derive a parameterized expression, the stratification effects are considered by introducing the turbulence damping coefficient ϕ_d, $\varepsilon_{sm}(z)=\phi_d\varepsilon_s(z)$ (van Rijn, 2007).

$$\phi_d=\phi_{fs}[1+(c_v/\phi_{s,\max})^{0.8}-2(c_v/\phi_{s,\max})^{0.4}] \tag{11}$$

with $\phi_{fs}=d_{50}/(1.5d_{sand})$, and $\phi_{fs}=1$ for $d_{50}\ge 1.5d_{sand}$. c_v is volume sediment concentration of solids, $\phi_{s,\max}$ = 0.65 = maximum bed concentration in volume.

2.3.4. Hindered settling

For sand, according to Richardson and Zaki (1954) and van Rijn (2007), the settling velocity in a fluid-sediment suspension can be determined as:

$$w_s=w_{s,0}(1-c_v)^n \tag{12}$$

For silt and very fine sand (Te Slaa et al., 2015):

$$w_s=w_{s,0}\frac{(1-c_v/\phi_{s,struct})^m(1-c_v)}{(1-c_v/\phi_{s,\max})^{-2.5\phi_{s,\max}}} \tag{13}$$

in which $w_{s,0}$ is settling velocity in clear water and the formula of van Rijn (2007) was employed; *n* is an exponent, varying from 4.6 to 2.3; $\phi_{s,struct}$ = 0.5 is the structural density, and *m* = 1-2.

2.3.5. Mobile bed effects

For fine sediment, the grain roughness ($2.5d_{50}$) is very small and the roughness enhanced by mobile bed effects is dominant. Camenen et al. (2009) proposed the Nikuradse's equivalent roughness by compiling many datasets,

$$\frac{k_s}{d_{50}} = 0.6 + 2.4\left(\frac{\theta}{\theta_{cr,ur}}\right)^{1.7} \tag{14}$$

in which θ is the Shields parameter, and $\theta_{cr,ur} = 0.115F_{rw}^{1.2} / [W_{s*}^{0.4}(s-1)^{0.3}]$ is the critical Shields parameter for the inception of the upper regime. $F_{rw} = u_m / \sqrt{g\delta}$ is the wave Froude number, where u_m is the maximum wave orbital velocity, $\delta = \sqrt{\upsilon T}$ is the thickness of the viscous (Stokes) layer, and *T* is the wave period. $W_{s*} = \left[(s-1)^2 / (g\upsilon)\right]^{1/3} w_s$ is the dimensionless settling velocity. If $\theta < \theta_{cr,ur}$, $k_s < 3d_{50}$, which corresponds approximately to the skin friction.

Then, combining above physical processes, the solution of Eq. (1) turns to:

$$\bar{c}(z) = \overline{c_a} e^{-G(z)} \text{ with } G(z) = \int_{z_a}^{z} \frac{w_s}{\phi_d \varepsilon_s(z)} dz \tag{15}$$

2.4. Materials

Experimental data of Dohmen Janssen et al. (2001), Havinga (1992), Horikawa et al. (1982), Li (2014), O'Donoghue and Wright (2004), Ribberink and Al-Salem (1995), van Rijn et al. (1993), Williams et al. (1998), Yao et al. (2015) and Zhou and Ju (2007) were used to study and verify the proposed expressions, as listed in Table 1. The bed forms in the verification cases included flat bed (sheet flow) and rippled bed; the flow dynamics included wave only cases and combined wave-current cases; and the sediment materials included silt and sand. The field data in Caofeidian sea area (Zuo et al., 2014) and Huanghua port sea area (Zhao and Han, 2007) in Bohai bay, China, were collected for evaluation, where the sediment concentrations were observed during several wave events in silt-dominant sea area.

Table 1

Collected experimental data for sediment concentration

Source	Flow dynamics	Wave motion	d_{50} (mm)	Bed form
Horikawa et al. (1982)	Wave	Oscillatory tunnel	0.20	Flat bed
Havinga (1992)	Wave+current	Wave flume	0.10	Rippled bed
van Rijn et al. (1993)	Wave+current	Wave flume	0.11-0.22	Rippled bed
Ribberink and Al-Salem (1995)	Wave	Oscillatory tunnel	0.21	Flat bed
Williams et al. (1998)	Wave	Wave flume	0.329	Rippled bed
Dohmen Janssen et al. (2001)	Wave+current	Wave flume	0.13-0.32	Flat bed
O'Donoghue and Wright (2004)	Wave	Oscillatory tunnel	0.15-0.28	Flat bed
Zhou and Ju (2007)	Wave	Wave flume	0.062-0.11	Rippled bed
Li (2014)	Wave	Wave flume	0.045-0.11	Rippled bed
Yao et al. (2015)	Wave and Wave+current	Wave flume	0.046-0.088	Rippled bed & flat bed
Zhao and Han (2007)	Wave+current	Field data	0.036	Flat bed
Zuo et al. (2014)	Wave+current	Field data	0.015	Flat bed

3. Time-averaged SSC profile over flat bed

3.1. Formulations

Substituting the expression of wave-related sediment diffusivity to Eq. (15), the distribution of sediment concentration under wave conditions was yielded,

$$\bar{c}(z)=\begin{cases}\overline{c_a}\left(\dfrac{z}{z_a}\right)^{-\alpha} & z_a < z \le z_1 \\ \overline{c_{z1}}\left(\dfrac{z-h'}{z}\dfrac{z_1}{z_1-h'}\right)^{\frac{\alpha}{a}} & z_1 < z < z_2 \\ \overline{c_{z2}}\exp\left[-\dfrac{\alpha}{\beta_s\delta_w}(z-z_2)\right] & z \ge z_2\end{cases} \tag{16}$$

in which, $\alpha=\dfrac{w_s}{\phi_d\kappa u_*'}$ = Rouse number (suspension number) over flat bed considering stratification effects, z_1 = max(z_a, $0.5\delta_w$), z_2 = max(z_a, $2.5\delta_w$), $\overline{c_{z1}}=\overline{c_a}\left(\dfrac{z_1}{z_a}\right)^{-\alpha}$, $\overline{c_{z2}}=\overline{c_{z1}}\left(\dfrac{z_2-h'}{z_2}\dfrac{z_1}{z_1-h'}\right)^{\frac{\alpha}{a}}$, and $h'=az_2/b$. From Eq. (16), it can be seen that the distribution of SSC is power law in the low part, Rouse type in the middle part and exponential law in the upper part. Iteration is needed when using this equation as the stratification effects and hindered settling are included. Fortunately, there were only 5-7 iterations according to the verification cases. The convergence condition was settled as

10^{-5} for the c, υ_t, w_s and ε_s between two steps, i.e., the maximum difference of every variable should be less than 10^{-5}.

Under combined wave-current conditions, the phase-averaged SSC profile was calculated by numerical procedure,

$$\frac{d\bar{c}}{dz} = -\frac{w_s \bar{c}(z)}{\phi_d \varepsilon_s(z)} \tag{17}$$

3.2. Verification

3.2.1. Experimental cases

The experimental datasets of Dohmen Janssen et al. (2001), Ribberink and Al-Salem (1995) and Yao et al. (2015) were collected to verify the SSC profile under flat bed conditions. Actually, existing experimental data for flat bed (sheet flow) are mainly for sand. One case for silt is Yao et al. (2015)'s experiment. In the case of s1-f3212 and s1-o3812 with d_{50} = 46 μm in combined wave-current conditions, the ripples were washed away and the SSC profile was measured (Yao et al., 2015). Fig. 7 to Fig. 9 show the verification of the experimental data, and the calculated value fit the measured data.

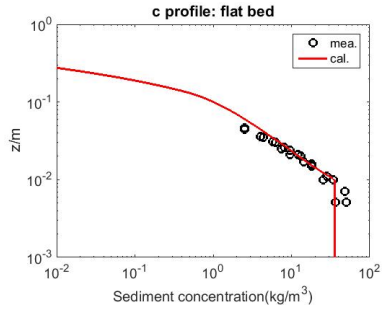

Fig. 7. Verification of the experimental data of Ribberink and Al-Salem (1995)

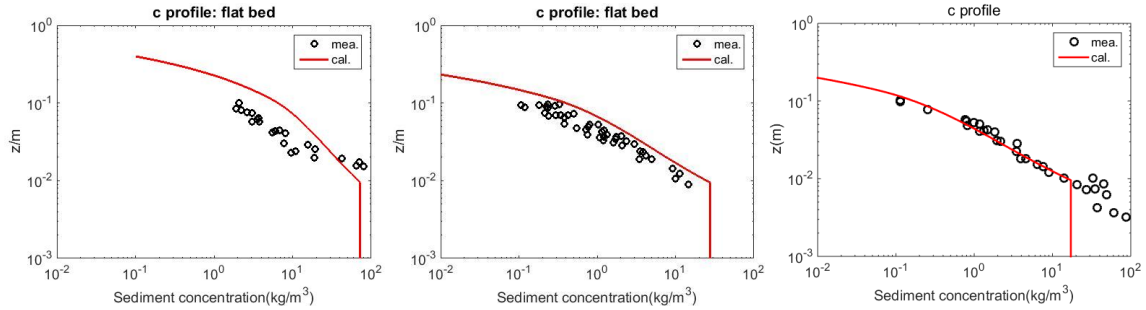

(a) d_{50} = 0.13 mm, u_c = 0.24 m/s (b) d_{50} = 0.21 mm, u_c = 0.23m/s (c) d_{50} = 0.32 mm, u_c = 0.26 m/s

Fig. 8. Verification of the experimental data of Dohmen Janssen et al. (2001) (u_c is current velocity)

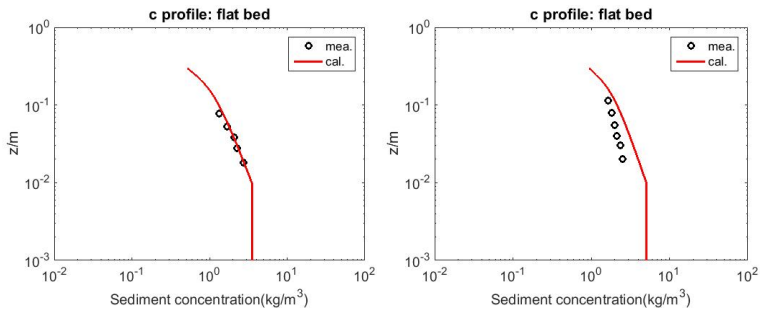

(a) case of s1-f3212 (d_{50} = 0.046 mm) (b) case of s1-o3812 (d_{50} = 0.046 mm)

Fig. 9. Verification of the experimental data of Yao et al. (2015)

3.2.2. Evaluation on field data

3.2.2.1. Caofeidian sea area

Fig. 10 shows the comparison of the calculated and measured concentration at 0.4 m above the bottom in Caofeidian sea area during several wave events (Zuo et al., 2014). The sediment median size is about 0.01~0.02 mm with average of 0.015 mm on the measurement site. Under calm conditions (with wave height < 0.5 m), sediment cannot be stirred up and sediment concentration was very low with the averaged value of only 0.05 kg/m^3. The sediment concentration increased during windy days. During November 16–17, when the maximum significant wave heights were 0.55–0.66 m, the measured peak SSC was 0.15 kg/m^3 with the average value of 0.08 kg/m^3; the significant wave heights of selected calculation at 16:00 on November 16, 5:00, 11:00 and 18:00 on November 17 were 0.62 m, 0.66 m, 0.24 m and 0.62 m respectively. During November 22–23 when the maximum significant wave height was about 0.6 m, the peak SSC was 0.26 kg/m^3 with the average value of 0.09 kg/m^3; the significant wave heights of selected calculation at 14:00 on November 22 and 17:00 on November 23 were 0.60 m and 0.55 m respectively. On November 28, when the maximum significant wave heights reached about 0.60–0.75 m, the peak SSC was 0.32 kg/m^3 and then decreased to below 0.1 kg/m^3; the significant wave heights of selected calculation at 11:00 and 15:00 on November 28 were 0.76 m and 0.67 m respectively. The wave period is about 3 seconds. It was assumed that the increase of sediment concentration may happen in some suitable conditions, e.g., when water depth was shallower and current velocity was larger. The calculation conditions were chosen as the shallowest water depth (2 m) and maximum flow velocity (0.57 m/s) on this site.

It has to be mentioned that, the measured wave data were available until November 15 due to battery failure. In order to supplement the wave data after November 15, several methods, such as the SMB method (Etemad-Shahidi et al., 2009) and Futaoijima method (Ministry of Transport of

China, 1998), were adopted to find out the significant wave heights from the observed wind speed data. Comparison of the estimated and measured wave heights during October 26 to November 15 shows that the Futaoijima method performed better and was chosen to recover the wave data. Details were presented in Zuo et al. (2014).

It can be seen that, though there is considerable discrepancy between the calculated and measured SSC peaks in Fig. 10, the magnitude is similar. The reason of the discrepancy may be as follows. First, this study is only for equilibrium concentration, while in the field, it is possible that sediment is suspended elsewhere (e.g., the shoal) and transported to this site, which is non-equilibrium. Second, the wave height was derived from wind speed by empirical methods, which might have caused the mismatch in phasing between waves (estimated) and concentrations (measured). Third, the sediment grain size Caofeidian is finer than the above experimental cases; however, silt is still the dominant part. We still need more data sets to verify fine sediment like in Caofeidian. Thus, we use "evaluation" instead of "verification", and only compare the order of magnitude of the SSC. Though there is large discrepancy in phase between the calculated and measured SSC, the magnitude is similar, around 0.1-0.3 kg/m^3.

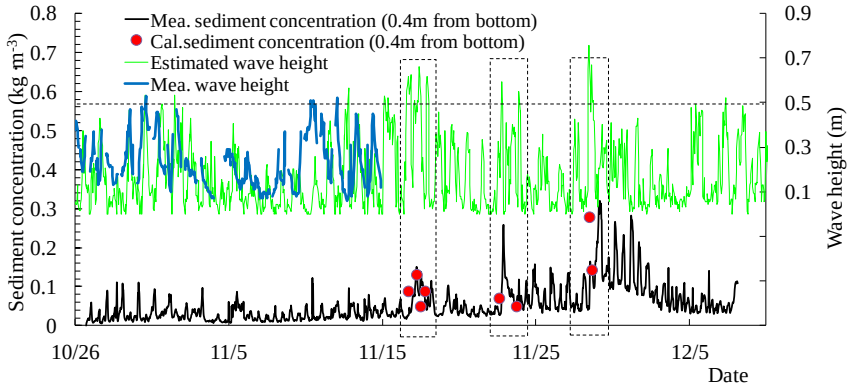

Fig. 10. Comparison of the calculated and measured concentration in Caofeidian sea area

3.2.2.2. Huanghua port sea area

According to the measured data in 2003 in Huanghua port sea area (Zhao and Han, 2007), we evaluate the performance of the parameterized expression. The "evaluation" is used here too, because of the missing of some details in the measured data, such as the process of the tidal level and the current velocities. The mean water depth is used as 6.4 m according to the bathymetry and mean tidal level. The medium size of bed material is 0.036 mm. Measurements show that high SSC occurs during storm surges, which causes heavy sudden siltation in navigation channels. The

average tidal current without winds is about 0.4 m/s, but the current velocities during windy days are not found. According to the wind speed, we estimated the mean wave-driven current velocity. The wind shear stress $\tau_s = \rho_a C_d U_{wind}{}^2$, where ρ_a is the density of air, C_d is the drag coefficient, U_{wind} is the wind velocity. The mean measured wind velocity during that event is about 14 m/s. The calculated τ_s is about 0.38 N/m^2. From $\bar{u} = \sqrt{\tau_s C^2 / (\rho g)}$, in which C is Chezy coefficient, the mean wind-induced current velocity $\bar{u}$ can be estimated as 0.4 m/s. The total mean velocity is estimated as sum of absolute value of the mean wind-induced current velocity and the mean tidal current velocity, 0.8 m/s. The input wave parameters were shown in Table 2.

Table 2

The input wave parameters in Huanghua port sea area

Parameters	a	b	c	d	e	f	g	h	i
Wave height (m)	2.28	2.22	2.29	2.21	2.49	1.81	1.52	0.87	2.30
Wave period (s)	6.00	5.70	6.63	6.23	5.83	5.32	4.70	4.70	6.00

Note: The wave parameters came from Zhao and Han (2007). The letters a to i represent the pictures of Fig. 11.

Fig. 11 shows the comparison of the calculated and measured SSC profiles in Huanghua port sea area during windy days. It can be seen that, during November 5 to November 6, 2003, the agreement between the calculated and measured concentration is quite good. After November 7, the wind speed as well as wave height became smaller; however, the SSC can still remain a certain value, because it needs time for sediment to settle down and the measured concentration is over-saturated (Fig. 11 (f), (g) and (h)). The term over-saturated means that the flow cannot carry the sediment load available. As the calculated value is an equilibrium one that could be seen as sediment capacity, it is reasonable that the calculated value is smaller than the measured one. It is one of the causes of the heavy deposition in navigation channel, i.e., the SSC is much higher than the sediment capacity after a wind, and sediment settles in the channels where the flow dynamics are normally weak.

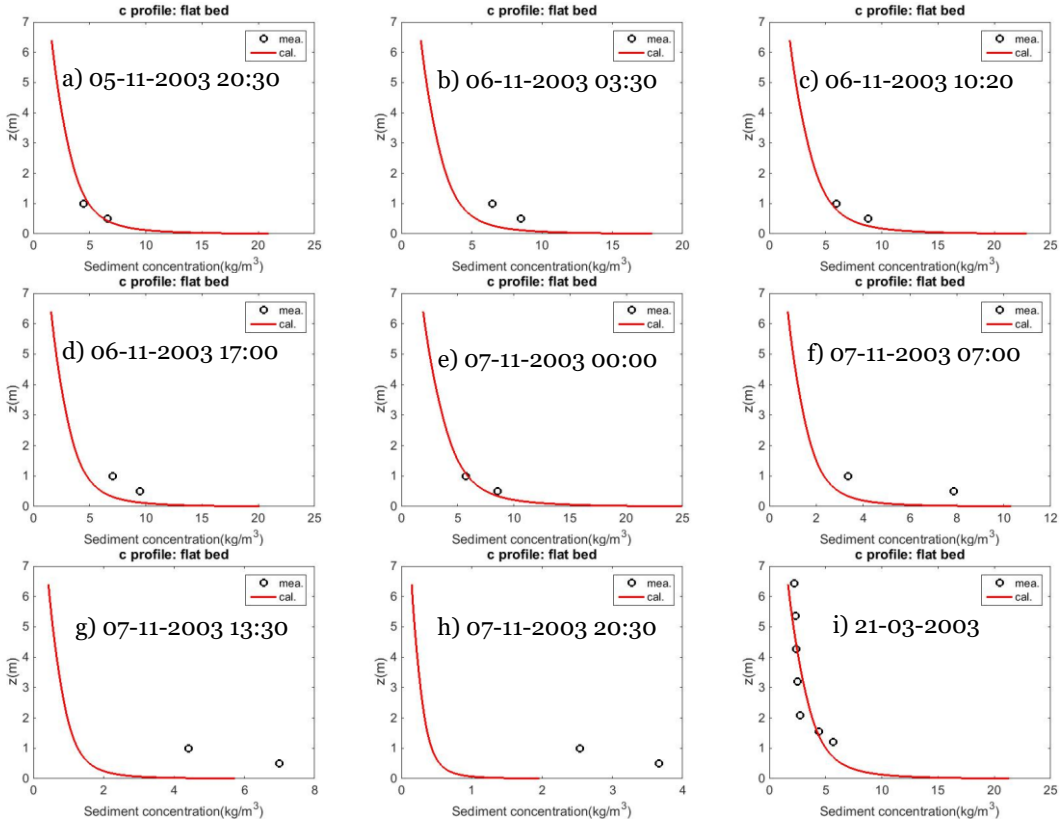

Fig. 11. Comparison of the calculated and measured SSC profiles in Huanghua port sea area during windy days in 2003

4. Time-averaged sediment concentration profile over rippled bed

4.1. Formulations

Substituting the expressions for the wave-related sediment diffusivity over rippled bed to Eq. (15), then, the distribution of SSC under wave conditions was yielded. However, the expression is too complex to integrate analytically when $\varepsilon_s(z)=\beta(z)\upsilon_t(z)/\sigma$ at $z>2\eta$ is applied. An average value $\overline{\beta}$ was used in the domain z_{1r} to z_{3r} from the perspective of practice,

$$\overline{\beta_i}=\frac{1}{\Delta z}\int_{z_i}^{z_{i+1}}\beta(z)dz \;=\; 4-\alpha_\beta[(z_{i+1}-2\eta)^{\gamma+1}-(z_i-2\eta)^{\gamma+1}]\frac{1}{\Delta z} \tag{18}$$

with $\alpha_\beta=\dfrac{1}{\gamma+1}\dfrac{3}{(h-2\eta)^\gamma}$ and $\Delta z=z_{i+1}-z_i$.

The final expression for sediment concentration profile over rippled bed under wave conditions:

$$\bar{c}(z)=\begin{cases}\overline{c_a}\exp[-\dfrac{w_s}{4\phi_d\overline{\upsilon_{tN}}}(z-z_a)] & z_a<z\le z_{1r}\\ \overline{c_{z1r}}(\dfrac{z}{z_{1r}})^{-\alpha_r} & z_{1r}<z\le z_{2r}\\ \overline{c_{z2r}}(\dfrac{z-h'}{z}\dfrac{z_{2r}}{z_{2r}-h'})^{\alpha_r/a_r} & z_{2r}<z<z_{3r}\\ \overline{c_{z3r}}d(z)^{\alpha_d} & z\ge z_{3r}\end{cases} \tag{19}$$

in which $\alpha_r=w_s/(\phi_d\overline{\beta}\kappa u_{v*})$ = Rouse number (suspension number) over rippled bed considering stratification effects, z_{1r} = max(z_a, 2η), z_{2r} = max(z_a, 2.5η), z_{3r} = max(z_a, 4.5η), $h'=a_r z_{3r}/b_r$,

$\overline{c_{z1r}}=\overline{c_a}\exp[-\dfrac{w_s}{4\phi_d\overline{\upsilon_{tN}}}(z_{1r}-z_a)]$, $\overline{c_{z2r}}=\overline{c_{z1r}}(\dfrac{z_{2r}}{z_{1r}})^{-\alpha_r}$ and $\overline{c_{z3r}}=\overline{c_{z2r}}(\dfrac{z_{3r}-h'}{z_{3r}}\dfrac{z_{2r}}{z_{2r}-h'})^{\alpha_r/a_r}$.

$d(z)=\dfrac{4(h-2\eta)-3(z-2\eta)}{4(h-2\eta)-3(z_{3r}-2\eta)}$ and $\alpha_d=\dfrac{w_s}{\phi_d\kappa u_{v*}}\dfrac{1}{b_{up}\eta}\dfrac{h-2\eta}{3}$.

Eq. (19) shows an exponential distribution in the vortex-dominant layer near the bottom and power-Rouse type distributions at the upper part. The expression has similar structure with Bolaños et al. (2012), who collected many experimental data and proposed the sand SSC profile formula by data fitting. Under combined wave-current conditions, the approach is the same for flat bed, i.e., by solving the numerical procedure of Eq. (17).

4.2. Verification

Some experimental datasets were collected to verify the mean SSC profile over rippled bed, see Table 1, including Havinga (1992), Li (2014), van Rijn et al. (1993), Yao et al. (2015) and Zhou and Ju (2007). These cases include sediment range of silt and sand, wave-only conditions and combined wave-current conditions. Fig. 12 - Fig. 16 show the calibration results.

It can be seen that, under wave-only conditions, the calculated sediment concentration agrees well with the measured data. The measured SSC profile can be considered as a fully developed equilibrium profile under wave-only conditions, because of the relatively small net current. However, under combined wave-current conditions (e.g., Fig. 12(c), Fig. 12(f), Fig. 13(b), Fig. 13(d), Fig. 16(g) and Fig. 16(h)), the calculated sediment concentration is larger than the measured value and the discrepancy increases with a stronger current. This is because the measured sediment concentration is non-equilibrium while the calculated concentrations is the equilibrium value.

Sufficient sediment source and a certain distance are needed to establish the equilibrium concentration when a current is added. The length of sediment section in flume experiments was normally not long enough to achieve equilibrium under combined wave-current or current conditions (Yao et al., 2015). For example, the length of the sediment bed was 15 m and 25 m in Yao et al. (2015)'s experiment and van Rijn et al. (1993)'s experiment, respectively, and it was still too short to develop equilibrium concentration when relatively strong currents were imposed.

The non-equilibrium concentration may be further simulated by a 2DV or 3D model considering longitudinal diffusive transport. However, despite of the discrepancies between the computed and measured data, the proposed equations are able to simulate a straighter SSC profile as the current velocity increases.

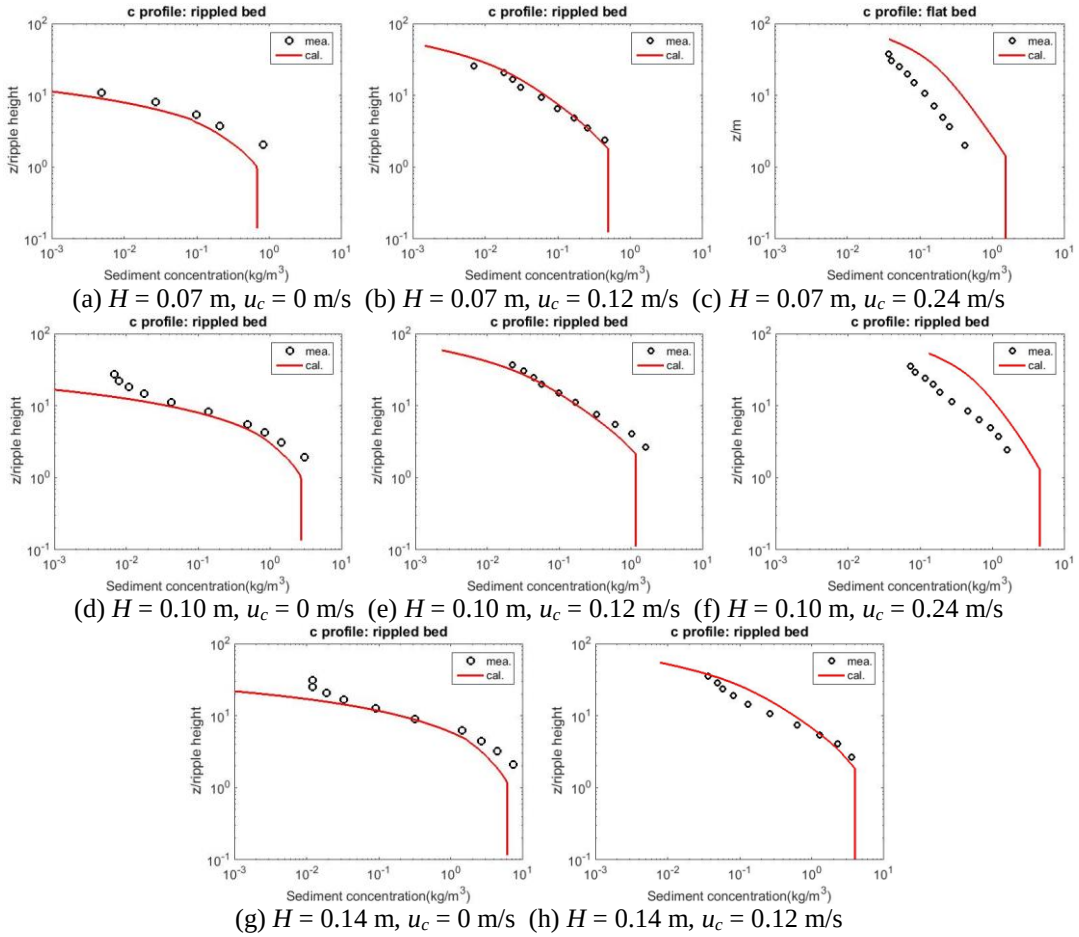

(a) H = 0.07 m, u_c = 0 m/s (b) H = 0.07 m, u_c = 0.12 m/s (c) H = 0.07 m, u_c = 0.24 m/s

(d) H = 0.10 m, u_c = 0 m/s (e) H = 0.10 m, u_c = 0.12 m/s (f) H = 0.10 m, u_c = 0.24 m/s

(g) H = 0.14 m, u_c = 0 m/s (h) H = 0.14 m, u_c = 0.12 m/s

Fig. 12. Verification of the experimental data of Havinga (1992) (H is wave height, h = 0.4 m, d_{50} = 100 μm)

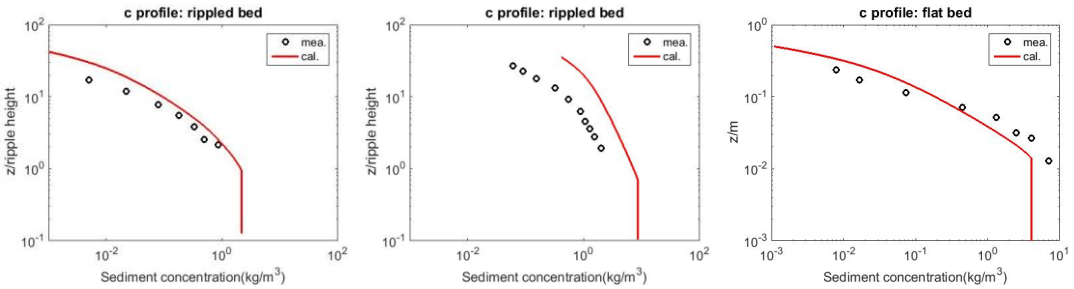

(a) *d1:* H = 0.1 m, u_c = 0.1 m/s (b) *d1:* H = 0.1 m, u_c = 0.35 m/s (c) *d1:* H = 0.18 m, u_c = 0.13 m/s

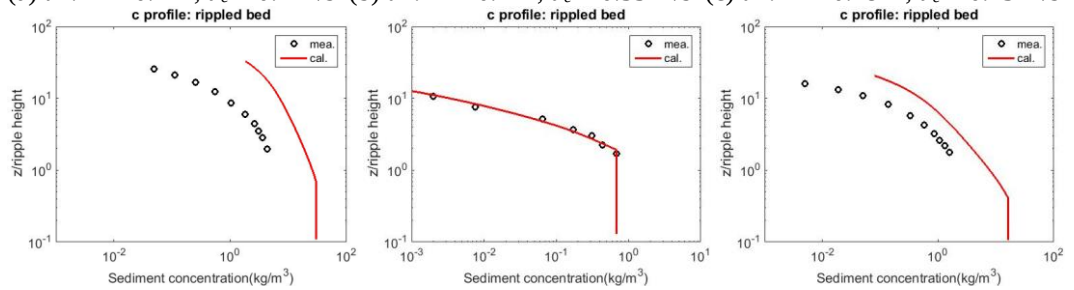

(d) *d1:* H = 0.18 m, u_c = 0.4 m/s (e) *d2:* H = 0.15 m, u_c = 0.13 m/s (f) *d2:* H = 0.15 m, u_c = 0.44 m/s

Fig. 13. Verification of the experimental data of van Rijn et al. (1993) (h = 0.4 m, *d1:* d_{50} = 110 μm and *d2:* d_{50} = 200-220 μm)

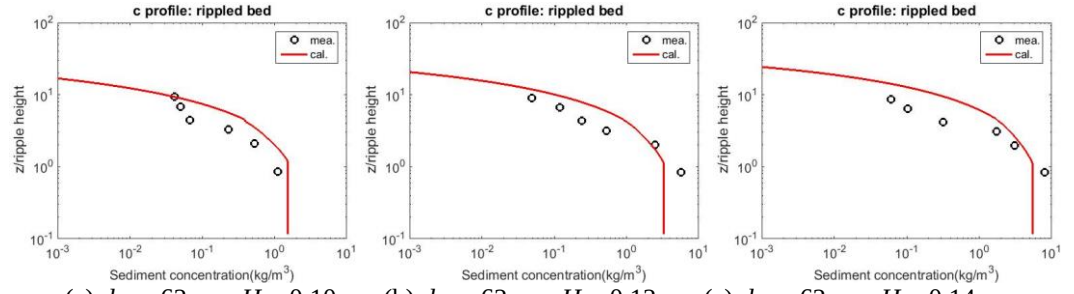

(a) d_{50} = 62 μm, H = 0.10 m (b) d_{50} = 62 μm, H = 0.12 m (c) d_{50} = 62 μm, H = 0.14 m

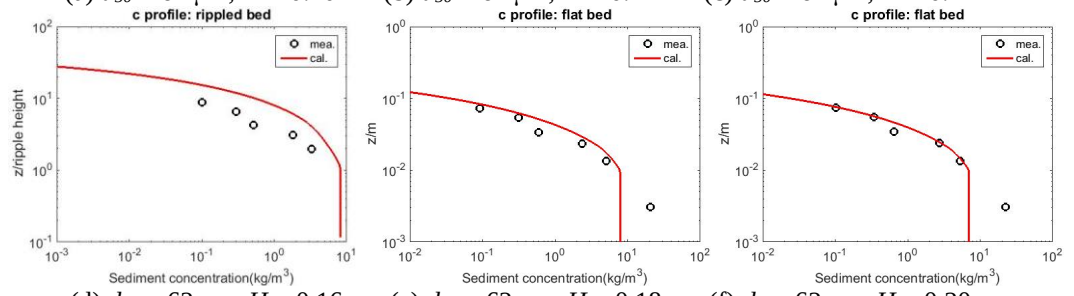

(d) d_{50} = 62 μm, H = 0.16 m (e) d_{50} = 62 μm, H = 0.18 m (f) d_{50} =62 μm, H = 0.20 m

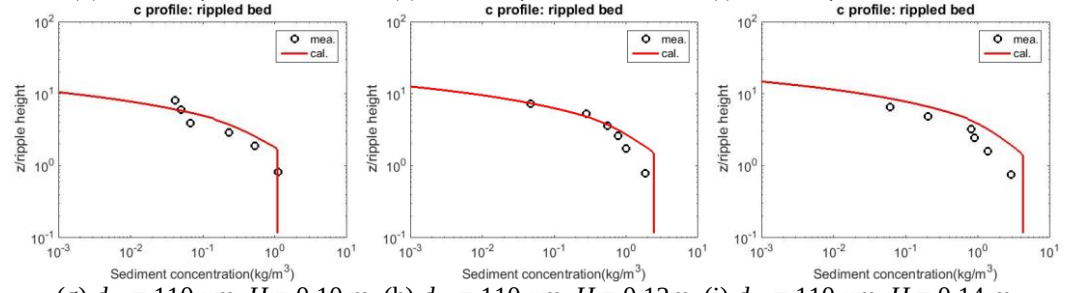

(g) d_{50} = 110 μm, H = 0.10 m (h) d_{50} = 110 μm, H = 0.12m (i) d_{50} = 110 μm, H = 0.14 m

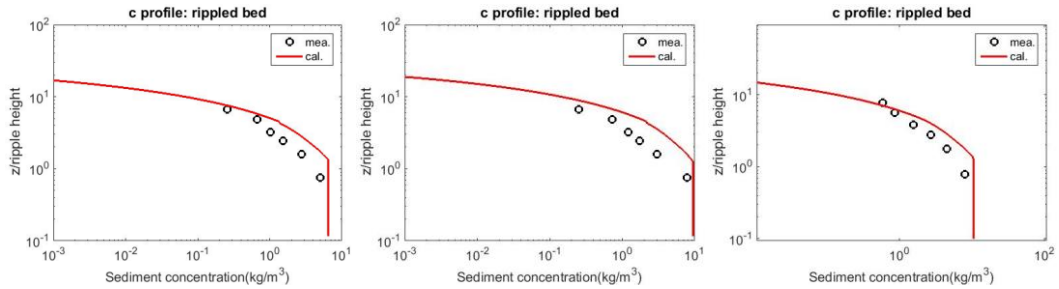

(j) d_{50} = 110 μm, H = 0.16 m (k) d_{50} = 110 μm, H = 0.18 m (l) d_{50} = 110 μm, H = 0.20 m

Fig. 14. Verification of the experimental data of Zhou and Ju (2007) (h = 0.5 m, T = 2 s, u_c = 0 m/s)

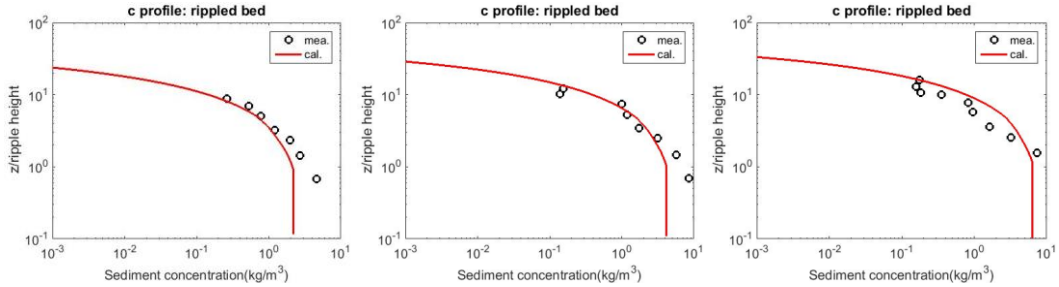

(a) d_{50} = 45 μm, H = 0.12 m (b) d_{50} = 45 μm, H = 0.15 m (c) d_{50} = 45 μm, H = 0.18 m

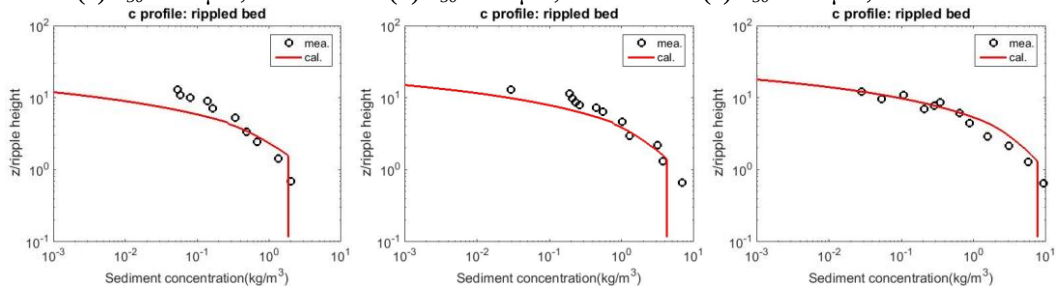

(d) d_{50} = 110 μm, H = 0.12 m (e) d_{50} = 110 μm, H = 0.15 m (f) d_{50} = 110 μm, H = 0.18 m

Fig. 15. Verification of the experimental data of Li (2014) (h = 0.5 m, T = 2 s, u_c = 0 m/s)

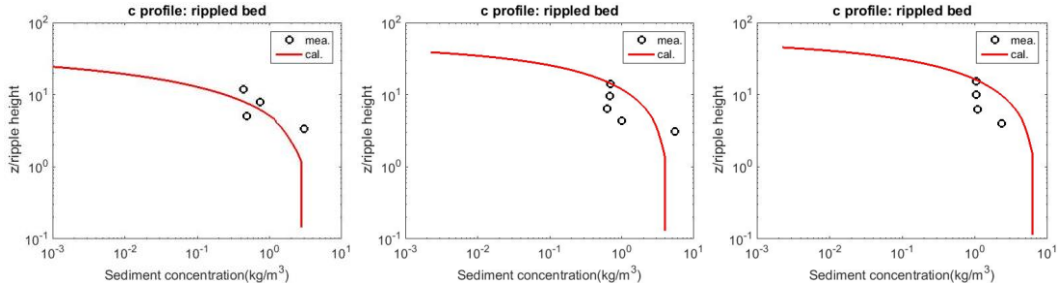

(a) *s1:* H = 0.09 m, u_c = 0 m/s (b) *s1:* H = 0.11 m, u_c = 0 m/s (c) *s1:* H = 0.13 m, u_c = 0 m/s

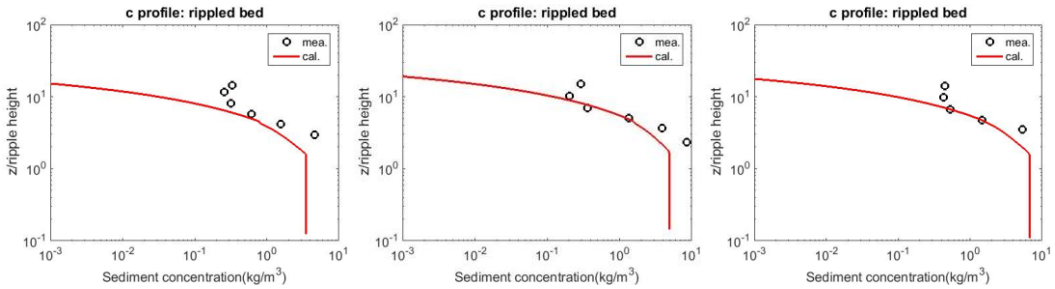

(d) *s2: H* = 0.09 m, u_c = 0 m/s (e) *s2: H* = 0.10 m, u_c = 0 m/s (f) *s2: H* = 0.12 m, u_c = 0 m/s

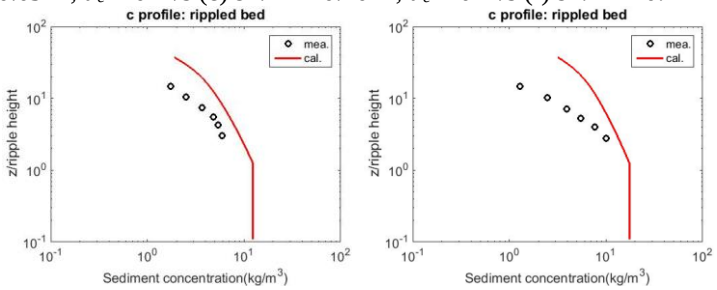

(g) *s2: H* = 0.11 m, u_c = 0.33 m/s (h) *s2: H* = 0.11 m, u_c = -0.39 m/s

Fig. 16. Verification of the experimental data of Yao et al. (2015) (*h* = 0.3 m, *T* = 1.5 s, *s1:* d_{50} = 44 μm, *s2:* d_{50} = 88μm)

5. Discussion

5.1. The SSC profile over rippled but hydrodynamically plane bed

The above results over rippled bed are only valid for vortex ripples, with ripple steepness larger than 0.12. For the lower ripple steepness, as the bed form is hydrodynamically plane (Davies and Thorne, 2005; van der Werf et al., 2006), the 'flat bed' method is used for SSC profiles. However, the roughness height is still calculated by the rippled bed method.

Fig. 17 shows verification of some experimental cases of Havinga (1992), van Rijn et al. (1993) and Zhou and Ju (2007) with low ripple steepness and Table 3 shows the experimental conditions. It can be seen that, the calculated sediment concentration profiles fit the measured data. The results indicate that the approaches can roughly represent the main physical background of this bed form. As this kind of bed type is a transition zone between vortex ripples and sheet flow, the turbulence diffusion is very complex and still needs further study.

Table 3
Some experimental cases over rippled bed forms with low ripple steepness

Case	d_{50} (μm)	u_m (m/s)	u_c (m/s)	Mobility number	Ripple height (m)	Ripple length (m)	Ripple steepness
Zhou and Ju (2007)	62	0.35-0.39	0.0	124-154	0.0058-0.0073	0.0638	0.091-0.115
Havinga (1992)	100	0.31	0.240	94.6	0.0079	0.0745	0.106
van Rijn et al. (1993)	111	0.35	0.131	76.8	0.0070	0.0680	0.103

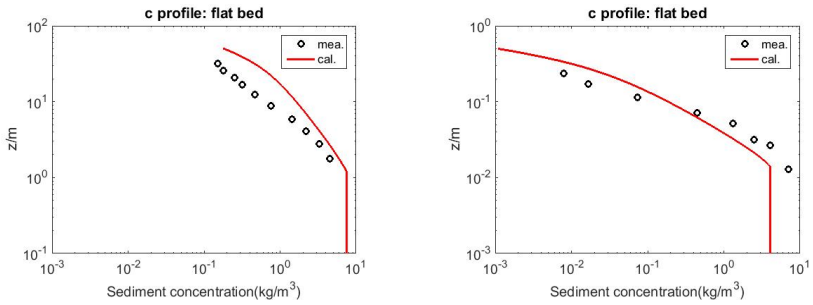

(a) Havinga (1992): H = 0.14 m, u_c = 0.24 m/s (b) van Rijn et al. (1993): H = 0.18 m, u_c = 0.13 m/s

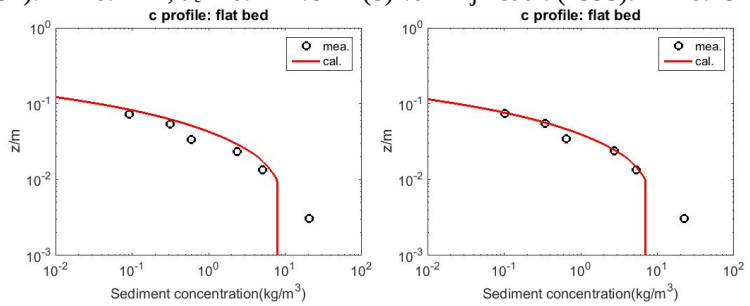

(c) Zhou and Ju (2007): d_{50} = 62 μm, H = 0.18 m (d) Zhou and Ju (2007): d_{50} = 62 μm, H = 0.20 m

Fig. 17. Verification of the experimental data of Havinga (1992), van Rijn et al. (1993) and Zhou and Ju (2007)

5.2. Comparison with other formulas

Two formulas for SSC profile were chosen to compare, the formula of van Rijn (2007) and Nielsen (1992). van Rijn (2007) proposed a distribution of sediment diffusivity, Eq. (20). The sediment concentration profile was derived from Eq. (20), considering the stratification effects and hindered settling.

$$\varepsilon_{s,w}=\begin{cases}\varepsilon_{s,w,bed} & z\le\delta_s\\ \varepsilon_{s,w,bed}+(\varepsilon_{s,w,\max}-\varepsilon_{s,w,bed})\left(\dfrac{z-\delta_v}{0.5h-\delta_v}\right) & \delta_s<z<0.5h\\ \varepsilon_{s,w,\max} & z\ge 0.5h\end{cases} \tag{20}$$

in which, $\varepsilon_{s,w,bed}=0.018\gamma_w\beta_w\delta_v U_{\delta,r}$ = wave-related sediment mixing coefficient near the bed; $U_{\delta,r}$ = representative near-bed peak orbital velocity based on significant wave height; $\beta_w=1+2(w_s/u_{*,w})^2$ with $\beta_w\le 1.5$; $u_{*,w}$ = wave-related bed-shear velocity; $\gamma_w=1+(H_s/h-0.4)^{0.5}$ = empirical coefficient related to wave breaking ($\gamma_w=1$ when $H_s/h<0.4$); H_s is significant wave height; $\varepsilon_{s,w,\max}=0.035\gamma_w hH_s/T$ with $\varepsilon_{s,w,\max}\le 0.05m^2/s$. The thickness of effective near-bed sediment mixing layer $\delta_v=2\gamma_w\delta_w$ with limits $0.1\le\delta_v\le 0.5m$.

$\delta_w = 0.36A_\delta(A_\delta / k_{s,w,r})^{-0.25}$ = thickness of wave boundary layer, A_δ = peak orbital excursion based on significant wave height; and $k_{s,w,r}$ = wave-related bed roughness.

Nielsen (1992) proposed a formula for SSC profile, Eq. (21), considering advection effects of ripples,

$$\bar{c}(z) = \overline{c_a} \exp[-\frac{1}{L_s}(z - z_a)] \tag{21}$$

in which, L_s is the vertical scale of the convective mixing process.

Fig. 18 shows comparison of the SSC profiles using different formulas. It can be seen that, all formulas could simulate the sediment concentration profile well in sand regime; however, in silt range, the distribution of sediment diffusivity of van Rijn (2007) over-estimated while Nielsen (1992) low-estimated the SSC profile. The formulas of van Rijn (2007) and Nielsen (1992) were derived for sand regime and worked well in their application scope. Actually, it is not suitable to compare these formulas in silt range without revising. The proposed expressions in this paper can simulate the sediment concentration profiles for both silt and sand reasonably.

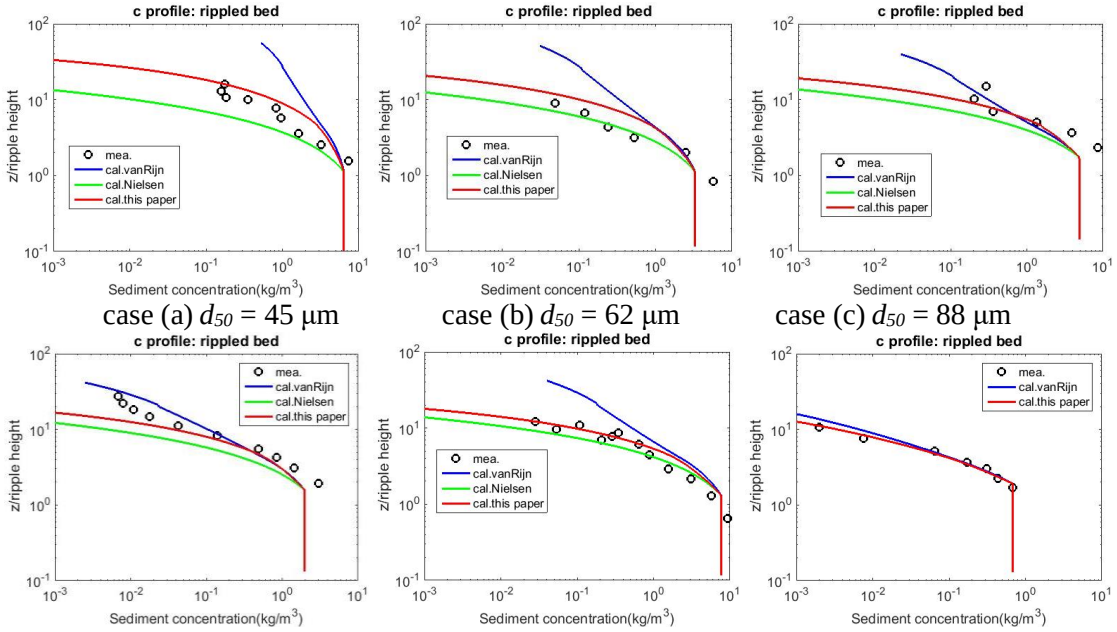

case (a) d_{50} = 45 μm case (b) d_{50} = 62 μm case (c) d_{50} = 88 μm

case (d) d_{50} = 100 μm case (e) d_{50} = 110 μm case (f) d_{50} = 223 μm

Fig. 18. Comparison of sediment concentration profile by different formulas (case (a): based on Li (2014)'s experiment with H = 0.18 m; case (b): based on Zhou and Ju (2007)'s experiment with H = 0.12 m; case (c): based on Yao et al. (2015)'s experiment with H = 0.10 m; case (d): based on Havinga (1992)'s experiment with H = 0.10 m; case (e): based on Li (2014)'s experiment with H = 0.18 m; case (f): based on van Rijn et al. (1993)'s experiment with H = 0.15 m and u_c = 0.13 m/s)

5.3. Sensitivity analysis on stratification effects and hindered setting velocity

5.3.1 The role of stratification effects

To investigate the stratification effects on SSC profile in silt regime, Fig. 19 presents the comparison of SSC profiles with ($\phi_d \neq 1$) and without stratification effects ($\phi_d = 1$), as well as comparison with measured data. Meanwhile, Fig. 20 shows the distribution of sediment diffusivity with and without stratification effects. In these figures, the median sediment grain size was in the range of 45 μm to 223 μm. As the stratification effects relate to sediment concentration as well, the cases which had similar magnitude order of the reference concentration, with 1~10 kg/m^3, were chosen.

Fig. 19 shows that the stratification effects have strong effects on finer sediment, and the effects are smaller when grain size is coarser, which is in line with common understanding. Comparison of the depth-averaged sediment concentration shows that (Fig. 21), the ratio of the average concentration in the study cases with and without stratification effects was 0.46, 0.61, 0.84, 0.86 and 0.93, for d_{50} = 45, 62, 88, 110 and 223 μm, respectively. Thus, stratification is a non-negligible factor for silt and very fine sand. The approaches employed here could automatically suggest the weights of the stratification effects on SSC with different grain sizes.

Considering stratification effects, iteration is needed during calculation to achieve a stable concentration. Turbulence diffusion supports sediment suspension, while settling and stratification effects decrease sediment concentration, thus there is a balance among these processes. The stratification effects do not reduce sediment concentration endlessly. According to the study cases in Fig. 19, steady values of sediment concentration, sediment diffusivity and damping coefficient can be achieved after 5-7 times iteration.

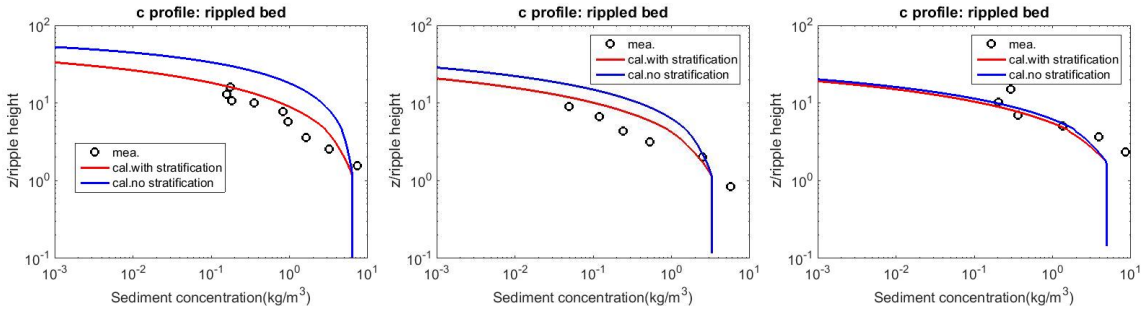

case (a) d_{50} = 45 μm case (b) d_{50} = 62 μm case (c) d_{50} = 88 μm

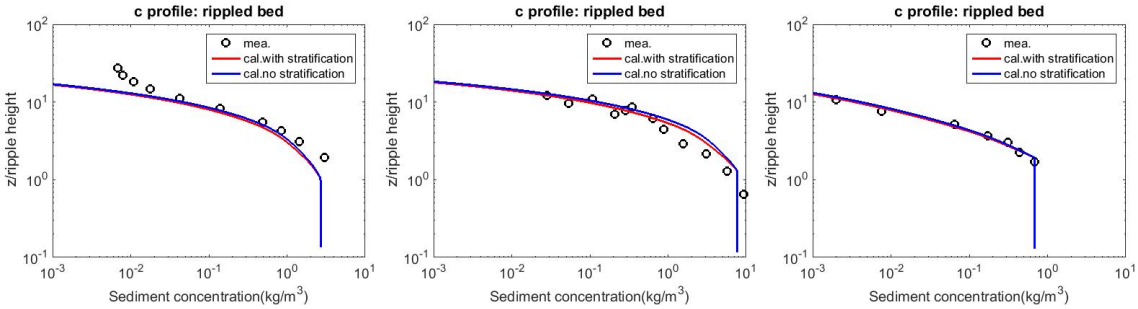

case (d) d_{50} = 100 μm case (e) d_{50} = 110 μm case (f) d_{50} = 223 μm

Fig. 19. Comparison of the calculated SSC profile with and without stratification effects (case (a): based on Li (2014)'s experiment with H = 0.18 m; case (b): based on Zhou and Ju (2007)'s experiment with H = 0.12 m; case (c): based on Yao et al. (2015)'s experiment with H = 0.10 m; case (d): based on Havinga (1992)'s experiment with H = 0.10 m; case (e): based on Li (2014)'s experiment with H = 0.18 m; case (f): based on van Rijn (1993)'s experiment with H = 0.15 m and u_c = 0.13 m/s)

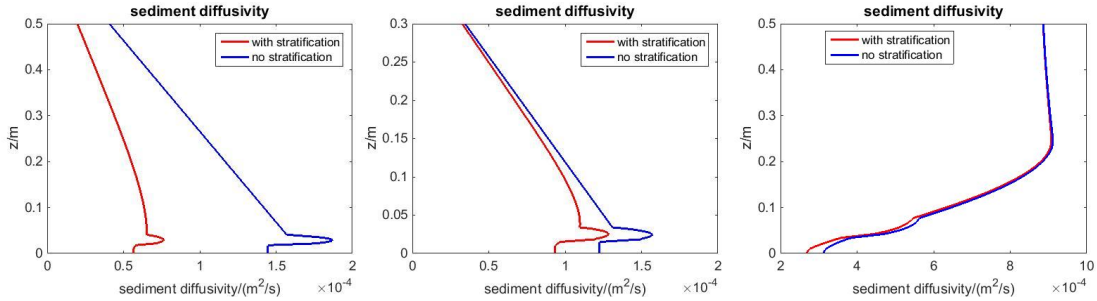

case (a) d_{50} = 45 μm case (c) d_{50} = 88 μm case (f) d_{50} = 223 μm

Fig. 20. Comparison of the calculated sediment diffusivity profiles with and without stratification effects

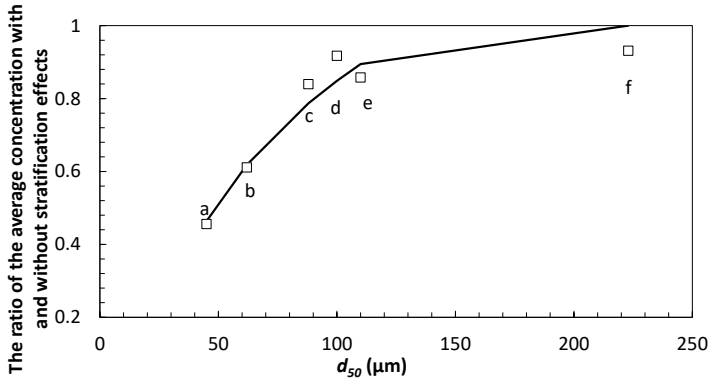

Fig. 21. The ratio of the average sediment concentration with and without stratification effects of the study cases

585 *5.3.2 The role of hindered settling velocity*

586 As hindered settling of silt has been studied extensively (e.g., Te Slaa et al. (2015)), we do not
587 study the mechanism of hindered settling velocity, but only give the sensitivity comparison with
588 and without hindered settling. Fig. 22 shows that, the effects of hindered settling velocity only
589 impact the SSC profiles when SSC is high, for which the SSC becomes higher due to lower settling
590 velocity. For case (a) (d_{50} = 0.13 mm) in Fig. 22, with the reference concentration of 72.5 kg/m^3,
591 the depth-averaged SSC is increased by about 6.2% with the effects of hindered settling velocity;
592 for case (b), with d_{50} = 0.32mm and the reference concentration of 17.2 kg/m^3, the changes of the
593 depth-averaged SSC is only about 1.5% and the hindered settling velocity has little effects on the
594 SSC profile. In case (c), which has finer sediment grain size and with the reference concentration
595 of 80.6 kg/m^3, the SSC is increased by 11.7% with the effects of hindered settling velocity. The
596 effects of hindered settling velocity are bigger with higher concentration and finer sediment, which
597 is in line with common understanding.

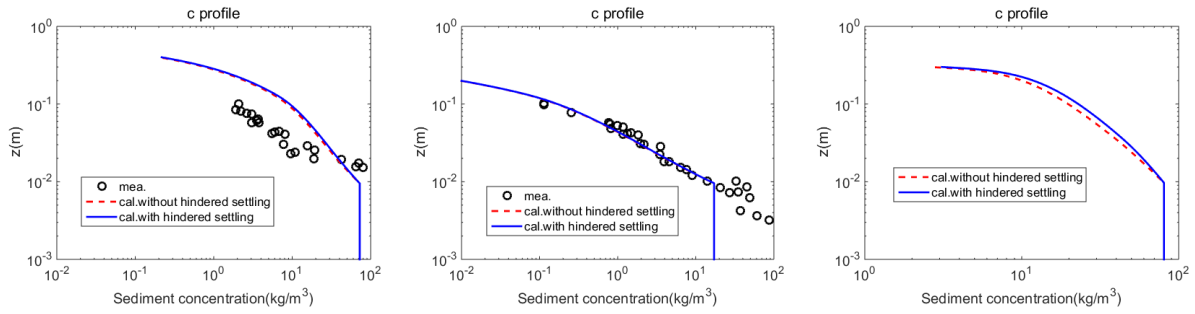

598

599 (a) (b) (c)

600 Fig. 22 Comparison of sediment concentration with and without hindered settling velocity ((a)
601 Dohmen Janssen et al. (2001), d_{50} = 0.13 mm, u_c = 0.24 m/s; (b) Dohmen Janssen et al. (2001), d_{50}
602 = 0.32 mm, u_c = 0.26 m/s; (c) d_{50} = 0.062 mm, u_m = 1.0 m/s, u_c = 0.6 m/s, h = 0.3m)

603 **6. Conclusion and remarks**

604 By solving the time-averaged diffusion equation for SSC and considering the effects of bed
605 forms, stratification, hindered settling and mobile bed, expressions for phase-averaged SSC profile
606 under wave conditions were proposed for silt and are applicable for sand as well. Under combined
607 wave-current conditions, numerical procedures were used for SSC profiles. A number of
608 experimental datasets as well as filed data were collected for verification and reasonable results
609 were obtained. The results are as follows:

610 Over flat bed, a toe-type distribution of wave-related sediment diffusivity was proposed. The
611 proposed SSC profile under wave conditions is power law in the low part, Rouse type in the middle

part and exponential distribution in the upper part, Eq. (16). Over rippled bed, a two-layer model was adopted (i.e., vortex-dominant layer and upper turbulence suspension layer). The proposed SSC profile under wave conditions is an exponential distribution in the vortex-dominant layer near the bottom and power-Rouse distributions at the upper part, Eq. (19). The results of verification show that the proposed expressions fit the measured data well.

Sediment suspension is a complex physical process, which is impacted by many factors. For example, in natural environments the mixtures of clay, silt and sand would affect sediment suspension. For silt dominant mixtures, the sediment grains which form rippled bed may differ from that in suspension. Generally, sediment grain size in rippled bed is coarser than d_{50}, while sediment grain size in suspension is smaller than d_{50}. This will affect the bed form dimension as well as the representative suspended sediment size, and thus the final SSC profile calculations. At this stage, this study focuses on uniform sediment and it is a future direction to study sediment mixtures.

The effects of bed forms on SSC are complicated, especially in the transition zone from rippled bed to plane bed, where the sediment suspension is far more deeply understood; more measured data and research are needed for the turbulence process, sediment diffusivity and roughness etc.

Selected notation

A	Wave amplitude	β	Adjusted parameter of sediment diffusivity
$\bar{c}$	Mean sediment concentration	β_s	Coefficient
$\overline{c_a}$	Time-averaged reference sediment concentration	β_z	Compaction coefficient
c_v	Volume sediment concentration of solids	δ_s	Bound water thickness
d	Diameter of bed material	δ_w	Thickness of wave boundary layer
d_{50}	Median size of sediment	ε	Turbulent dissipation
D_*	Dimensionless particle size	ε_k	Cohesive force coefficient
g	Gravitational acceleration	ε_s	Sediment diffusivity
h	Water depth	$\varepsilon_{s,c}$	Current-related sediment diffusivity coefficient
H	Wave height	$\varepsilon_{s,w}$	Wave-related sediment diffusivity coefficient
k	Turbulent kinetic energy	$\varepsilon_{s,cw}$	Combined sediment diffusivity coefficient of waves and currents
k_s	Roughness height	ϕ_d	Damping coefficient

$\mathrm{Re}\,d_*$	Non-dimensional sediment Reynolds number	$\phi_{s,struct}$	Structural density
s	Relative density	$\phi_{s,\max}$	Maximum density
T	Wave period	η	Ripple height
u_c	Mean current velocity	κ	Kaman number
u_m	Maximum wave orbital velocity	λ	Ripple length
u_*	Shear velocity	θ	Shields number
u_*'	Effective mean wave shear velocity	θ_{zc}	Revised critical Shields number (Incipience number)
u_{*_c}	Current-related shear velocity	υ	Kinematic viscosity coefficient
u_{*_w}	Wave maximum shear velocity	υ_t	Eddy viscosity
u_{wc}	Velocity of combined wave-current	$\overline{\upsilon_{tN}}$	Eddy viscosity in vortex-dominant layer
w_s	Settling velocity	ρ	Water density
$w_{s,0}$	Settling velocity in clear fluid	σ	Prandtl-Schmidt number
z	Vertical coordinate from flat bed or ripple crest level	τ_c	Critical shear stress
z_a	Reference height	ψ	Mobility number
α	Rouse number over flat bed considering stratification effects	ω	Wave frequency
α_r	Rouse number over rippled bed considering stratification effects		

Acknowledgments

The study is financially supported by National Key R&D Program of China (2016YFC0402107 and 2016YFC0402303), National Natural Science Foundation of China (NSFC) (Grant No. 51520105014 and 51509160) and the Joint Research Project of The Netherlands Organization for Scientific Research (NWO) - NSFC (Grant No. 51061130546).

References

Bagnold, R.A. and Taylor, G., 1946. Motion of waves in shallow water. Interaction between waves and sand bottoms, Proceedings of the Royal Society of London. Series A. Mathematical and Physical Sciences, pp 1-15.

Bolaños, R., Thorne, P.D. and Wolf, J., 2012. Comparison of measurements and models of bed stress, bedforms and suspended sediments under combined currents and waves. Coastal Engineering, 62, 19-30.

Camenen, B., Larson, M. and Bayram, A., 2009. Equivalent roughness height for plane bed under oscillatory flow. Estuarine Coastal & Shelf Science, 81(3), 409-422.

Cao, Z.D., Yang, S.S. and Yang, H., 2009. Definition of silt-sandy beach and its characteristics of sediment movement. Port & Waterway Engineering, (5), 1-4 (in Chinese with English abstract).

Coleman, N.L., 1969. A new examination of sediment suspension in open channels. Journal of Hydraulic Research, 7(1), 69-82.

Davies, A.G. and Thorne, P.D., 2005. Modeling and measurement of sediment transport by waves in the vortex ripple regime. Journal of Geophysical Research: Oceans (1978–2012), 110(C5).
Davies, A.G. and Villaret, C., 1999. Eulerian drift induced by progressive waves above rippled and very rough beds. Journal of Geophysical Research: Oceans, 104(C1), 1465-1488.
Davies, A.G. and Villaret, C., 2002. Prediction of sand transport rates by waves and currents in the coastal zone. Continental Shelf Research, 22(18), 2725-2737.
Dohmen Janssen, C.M., Hassan, W.N. and Ribberink, J.S., 2001. Mobile‐bed effects in oscillatory sheet flow. Journal of Geophysical Research: Oceans (1978–2012), 106(C11), 27103-27115.
Etemad-Shahidi, A., Kazeminezhad, M.H. and Mousavi, S.J., 2009. On the prediction of wave parameters using simplified methods. Journal of Coastal Research, Special Issue 56: 505-509.
Grant, W.D. and Madsen, O.S., 1986. The continental-shelf bottom boundary layer. Annual Review of Fluid Mechanics, 18(1), 265-305.
Guizien, K., M. Dohmen Janssen and G. Vittori, 2003. 1DV bottom boundary layer modeling under combined wave and current: Turbulent separation and phase lag effects. Journal of Geophysical Research: Oceans (1978–2012), 108(C1), 3016.
Havinga, F.J., 1992. Sediment concentrations and sediment transport in case of irregular non-breaking waves with a current. Delft University of Technology, Delft, the Netherlands.
Horikawa, K., Watanabe, A. and Katori, S., 1982. Sediment transport under sheet flow condition. Coastal Engineering Proceedings, 1(18), 1335-1352.
Jayaratne, M.P.R., Rahman, M.R. and Shibayama, T., 2015. A cross-shore beach profile evolution model. Coastal Engineering Journal, 5670(4), 56-101.
Jayaratne, M.P.R., Srikanthan, S. and Shibayama, T., 2011. Examination of the suspended sediment concentration formulae using full-scale rippled bed and sheet-flow data. Coastal Engineering Journal, 53(04), 451-489.
Li, S., 2014. Turbulent structure and sediment alluvial process in wave-current boundary layer, Nanjing Hydraulic Research Institute, Nanjing (in Chinese).
Li, Z. and A.G. Davies, 1996. Towards predicting sediment transport in combined wave-current flow. Journal of Waterway, Port, Coastal, and Ocean Engineering, 122(4), 157-164.
Liu, Q., 2007. Analysis of the vertical profile of concentration in sediment-laden flows. International Conference on the Art of Resisting Extreme Natural Forces, pp 355-362.
Lundgren, H., 1972. Turbulent currents in the presence of waves. Proc 13th ICCE, Vancouver, ASCE, pp 623-634.
Mehta, A.J. and Lee, S., 1994. Problems in linking the threshold condition for the transport of cohesionless and cohesive sediment grain. Journal of Coastal Research, 10(1), 170-177.
Ministry of Transport of China, 1998. Code of Hydrology for Sea Harbour, JTJ 213-98. China Communication Press, Beijing (in Chinese).
Nielsen, P., 1992. Coastal bottom boundary layers and sediment transport. Advanced Series on Ocean Engineering, 4. World scientific, Singapore.
Nielsen, P., 1995. Suspended sediment concentration profiles. Appl. Mech. Rev, 48(9), 564-569.
O'Donoghue, T. and Wright, S., 2004. Flow tunnel measurements of velocities and sand flux in oscillatory sheet flow for well-sorted and graded sands. Coastal Engineering, 51(11), 1163-1184.

O'Donoghue, T., Doucette, J.S., Van der Werf, J.J. and Ribberink, J.S., 2006. The dimensions of sand ripples in full-scale oscillatory flows. Coastal Engineering, 53(12), 997-1012.
Ravindra Jayaratne, M.P. and Shibayama, T., 2007. Suspended sediment concentration on beaches under three different mechanisms. Coastal Engineering Journal, 49(04), 357-392.
Ribberink, J.S. and Al-Salem, A.A., 1995. Sheet flow and suspension of sand in oscillatory boundary layers. Coastal Engineering, 25(3), 205-225.
Richardson, J.F. and Zaki, W.N., 1954. Sedimentation and fluidization: Part I. Transactions of the Institution of Chemical Engineers, 32, 35-53.
Roberts, J., Jepsen, R., Gotthard, D. and Lick, W., 1998. Effects of particle size and bulk density on erosion of quartz particles. Journal of Hydraulic Engineering, 124(12), 1261-1267.
Rouse, H., 1937. Modern conceptins of the mechanics of turbulence. Pesticide & Venom Neurotoxicity, 7(3), 1-4.
Sato, S., Mimura, N. and Watanabe, A., 1985. Oscillatory boundary layer flow over rippled beds. Coastal Engineering 1984, 2293-2309.
Sleath, J.F.A., 1982. The Suspension of sand by waves. Journal of Hydraulic Research, 20(5), 439-452.
Soulsby, R., 1997. Dynamics of marine sands: A manual for practical applications. Thomas Telford.
Stevens, R.L., 1991. Grain-size distribution of quartz and feldspar extracts and implications for flocculation processes. Geo-Marine Letters, 11(3), 162-165.
Te Slaa, S., He, Q., van Maren, D.S. and Winterwerp, J.C., 2013. Sedimentation processes in silt-rich sediment systems. Ocean Dynamics : Theoretical, Computational and Observational Oceanography, 63(4), 399-421.
Te Slaa, S., van Maren, D.S., He, Q. and Winterwerp, J.C., 2015. Hindered settling of silt. Journal of Hydraulic Engineering, 141(9), 04015020-1-13.
Thorne, P.D. and Hanes, D.M., 2002. A review of acoustic measurement of small-scale sediment processes. Continental Shelf Research, 22(4), 603-632.
Thorne, P.D., Williams, J.J. and Davies, A.G., 2002. Suspended sediments under waves measured in a large-scale flume facility. Journal of Geophysical Research: Atmospheres, 107(C8), 3178.
Umeyaina, M., 1992. Vertical distribution of suspended sediment in uniform open-channel flow. Journal of Hydraulic Engineering, 118(6), 936-941.
van der A, D.A., 2005. 1DV modelling of wave-induced sand transport processes over rippled beds, University of Twente, Enschede, The Netherlands.
van der Werf, J.J., Ribberink, J.S., O'Donoghue, T. and Doucette, J.S., 2006. Modelling and measurement of sand transport processes over full-scale ripples in oscillatory flow. Coastal Engineering, 53(8), 657-673.
Van Maren, D.S., Winterwerp, J.C., Wang, Z.Y. and Pu, Q., 2009. Suspended sediment dynamics and morphodynamics in the Yellow River, China. Sedimentology, 56(3), 785-806.
van Rijn, L.C., 1993. Principles of sediment transport in rivers, estuaries and coastal seas, 1006. Aqua publications Amsterdam.
van Rijn, L.C., 2007. Unified view of sediment transport by currents and waves. II: Suspended transport. Journal of Hydraulic Engineering, 133(6), 668-689.
van Rijn, L.C., Nieuwjaar, M.W., van der Kaay, T., Nap, E. and van Kampen, A., 1993. Transport of fine sands by currents and waves. Journal of Waterway, Port, Coastal, and Ocean Engineering, 119(2), 123-143.

Williams, J.J., Bell, P.S., Coats, L.E., Hardcastle, P.J., Humphrey, J.D., Moores, S.P., Thorne, P.D. and Trouw, K., 1998. Evaluation of field equipment used in studies of sediment dynamics, Proudman Oceanogr. Lab., Birkenhead, UK.

Winterwerp, J.C., 2006. Stratification effects by fine suspended sediment at low, medium, and very high concentrations. Journal of Geophysical Research: Oceans, 111, C05012.

Winyu, R. and Shibayama, T., 1995. Suspended sediment concentration profiles under non-breaking and breaking waves. Coastal Engineering 1994, 2813-2827.

Yao, P., Su M., Wang, Z.B., van Rijn, L.C., Zhang, C.K., Chen, Y.P. and Stive, M.J., 2015. Experiment inspired numerical modeling of sediment concentration over sand-silt mixtures. Coastal Engineering, 105, 75-89.

Zhang, C., Zheng, J., Wang, Y., Zhang, M., Jeng, D. and Zhang, J., 2011. A process-based model for sediment transport under various wave and current conditions. International Journal of Sediment Research, 26(4), 498-512.

Zhao, Q. and Han, H., 2007. Siltation mechanisms of Huanghua Port and 3D characteristics of nearshore suspended sediment concentration under waves. Journal of Waterway and Harbor, 28(2), 77-80 (in Chinese with English abstract).

Zheng, J., Li, R.J., Feng, Q. and Lu S.S., 2013. Vertical profiles of fluid velocity and suspended sediment concentration in nearshore. International Journal of Sediment Research, 28(3), 406–412.

Zhou, Y. and Ju, L., 2007. Test study on the characteristics of a wind-flow-wave flume and sediment movement under wave conditions, Nanjing hydraulic research institute, Nanjing (in Chinese).

Zuo, L., Lu, Y., Wang, Y. and Liu, H., 2014. Field observation and analysis of wave-current-sediment movement in Caofeidian sea area in the Bohai Bay, China. China Ocean Engineering, 28(3), 331-348.

Zuo, L., Roelvink, D., Lu, Y. and Li, S., 2017. On incipient motion of silt-sand under combined action of waves and currents. Applied Ocean Research, 69, 116-125.

Zuo L., Roelvink D., Lu Y., Wang H., 2018. Modelling and analysis on high sediment concentration layer of fine sediments under wave-dominated conditions. Coastal Engineering, 140: 205-231.

Zyserman, J.A. and Fredsøe, J., 1994. Data analysis of bed concentration of suspended sediment. Journal of Hydraulic Engineering, 120(9), 1021-1042.